Title	Effect of annealing on the development of fully transparent ternary V-O-Na-Si mixed metal oxide thin films from polymer-assisted dip-coated V2O5
Authors	O'Hanlon, Sally;Glynn, Colm;O'Dwyer, Colm
Publication date	2015-10-07
Original Citation	O'Hanlon, S., Glynn, C. and O'Dwyer, C. (2016) 'Effect of Annealing on the Development of Fully Transparent Ternary V-O-Na-Si Mixed Metal Oxide Thin Films from Polymer-Assisted Dip-Coated V2O5', ECS Journal of Solid State Science and Technology, 5(1), pp. R3100-R3106. doi:10.1149/2.0141601jss
Type of publication	Article (peer-reviewed)
Link to publisher's version	10.1149/2.0141601jss
Rights	© The Author(s) 2015. Published by ECS. This is an open access article distributed under the terms of the Creative Commons Attribution Non-Commercial No Derivatives 4.0 License (CC BY-NC-ND, http://creativecommons.org/licenses/by-nc-nd/4.0/), which permits non-commercial reuse, distribution, and reproduction in any medium, provided the original work is not changed in any way and is properly cited. For permission for commercial reuse, please email: oa@electrochem.org. [DOI: 10.1149/2.0141601jss] All rights reserved. - http://creativecommons.org/licenses/by-nc-nd/4.0/
Download date	2024-04-26 18:42:12
Item downloaded from	https://hdl.handle.net/10468/5485

University College Cork, Ireland
Coláiste na hOllscoile Corcaigh

JSS Focus Issue on Novel Applications of Luminescent Optical Materials

Effect of Annealing on the Development of Fully Transparent Ternary V-O-Na-Si Mixed Metal Oxide Thin Films from Polymer-Assisted Dip-Coated V_2O_5

Sally O'Hanlon,[a] Colm Glynn,[a,*] and Colm O'Dwyer[a,b,,z]**

[a]*Department of Chemistry, University College Cork, Cork T12 YN60, Ireland*
[b]*Micro-Nano Systems Centre, Tyndall National Institute, Lee Maltings, Cork T12 R5CP, Ireland*

Both transparent oxides and transparent conductive oxides are of particular research interest for future applications in flexible, optically transparent thin film transistors and luminescent devices. We report the formation of a transparent oxide material based on the interdiffusion of Na-O and Si-O species with dip-coated V_2O_5 thin films on a borosilicate glass substrate. The deposition process used a facile solution processed dip-coating technique in the high-rate draining regime. Liquid precursors of vanadium alkoxide and alkoxide-polyethylene glycol mixtures were used for thin film deposition. We examine the effect of annealing condition on the phase conversion process, morphology and optical transmittance due to the conversion of the V_2O_5 films to completely transparent ternary mixed metal oxide thin films. The work also examines the role of polymer-assisted deposition on the development of the V-O-Na-Si transparent thin films during different annealing conditions. Polymer-assisted V_2O_5 thin films on glass are shown to convert to optically clear thin films during annealing, with a transparency >95% across the visible spectrum, and a blue-shift of the absorption edge to maintain >90% transparency at 380 nm.
 [DOI: 10.1149/2.0141601jss]

Manuscript submitted July 31, 2015; revised manuscript received September 23, 2015. Published October 7, 2015. *This paper is part of the JSS Focus Issue on Novel Applications of Luminescent Optical Materials.*

Thin film transistors are the fundamental building blocks for state-of-the-art microelectronics[1] and metal oxide materials are critical for channel materials and transparent contacts in many of the devices. Transparent conductive oxides[2] (TCO) and transparent thin films (TTF) are widely used in optoelectronic applications as they offer transparency across a broadband frequency range, or indeed in specific spectral regions while maintaining some properties of a metallic conductor in addition to semiconducting behavior in many cases.[3] These properties make them ideal for incorporation into devices such as thin film transistors (TFT),[1,4] photovoltaics[5] and electrochromic windows,[6–9] and optical coatings as pertinent examples. Lower-cost precursor routes that lead to TCOs are appealing, particularly for TFT and photovoltaic devices, since they are solution-processable, do not require the use of high-vacuum processing methods and in principal may allow coating of non-planar substrates. TFTs using oxide semiconductors have positive attributes such as high field effect mobility, wide band gaps, can be grown by many methods, and function in an amorphous state. The range of oxide compositions may widen with the use of liquid-based precursors for solution-processed deposition of the coatings.[10]

Transition metal oxides have a controllable electrical conductivity, from almost insulating to degenerately semiconducting,[11] with previous work demonstrating that conductivity alterations are possible through additive selection.[12] Transition metal oxides are also an area of interest owing to the wide variety of possible elemental compositions and the large range of crystal structures possible, highlighting their potential use in many fields with particular emphasis on emerging transparent electronics. Many new applications of these thin films continue to be critical for the electronic,[1] energy storage,[13] optoelectronic[9,11,14–16] and photovoltaic[16–18] industries with new areas and applications under research each year. With an increasing range of potential applications, the importance of rapid thin film deposition over large areas is of greater importance, with solution processed techniques a strong candidate to fill this technological need.[19,20]

Spin- and dip-coating are two solution processed techniques which are well understood and capable of rapidly depositing a variety of thin films over large areas.[21] Unlike other deposition methods that require more complex processing equipment, such as sputtering or physical/chemical vapor (PVD, CVD) methods, spin- and dip-coating are cost-effective with a long history of use within both academia and industry.[22] Dip-coating offers a method of coating any shape of substrate to enable new applications in flexible, wearable and plastic electronics. A long sought-after goal for use in modern transparent devices is a material designed at molecular level that is solution processable and forms a semiconductor that has high mobility with controllable transparency in a variety of wavelength ranges (UV, visible or infrared) without a large detrimental effect on the electrical conductivity. Transparent TFT are crucial for next generation display and interactive technologies, but in some cases limited by expensive production methods, and by a limited range of new materials that are processable outside industrial settings.

Another factor affecting recent interest in TCO research is the search for an Indium-free alternative to high-performance metal oxides. An In-free fabrication of a low-temperature TCO that does not suffer from reduced charge carrier mobility and the ability to be deposited on flexible substrates while retaining optical transparency remains a technical goal.

Vanadium oxides (VO) are a well-known and a popular choice in a large variety of electrical, optical and energy storage applications. The popularity of VO materials is due in part to the many materials that can be formed due to the large variety of oxidative states and structures which are available: VO (cubic), VO_2 (monoclinic), V_2O_3 (monoclinic) and V_2O_5 (orthorhombic) form,[23] with each material having unique material characteristics. VO materials are the focus of many research areas as they have practical applications in critical temperature sensors[24], light detectors, catalysts,[25] photovoltaics,[5] inverse opal materials,[26] electrodes,[27] intercalation devices[12,28] and lithium ion batteries.[29–31]

Many methods can be employed in the formation of VO materials, particularly in solution processed methods where a range of metallorganic and inorganic precursors are available that can be stored and used for long periods, thus increasing their usefulness

*Electrochemical Society Student Member.
**Electrochemical Society Active Member.
[z]E-mail: c.odwyer@ucc.ie

in thin film and coating research.[32] V_2O_5 has thermochromic and electrochromic properties under continual investigation as it is an n-type semiconductor material with a wide bandgap.[33] However, rational doping with several species to alter the optical and electrical characteristics can be complex, particularly for liquid precursors where inorganic molecular design of mixed metal species may be required. Here, we investigate the optoelectronic characteristics of completely transparent ternary mixed metal oxide thin films formed by diffusion of substrate species into uniform V_2O_5 films produced by high-rate dip coating from an alkoxide precursor solution, and also form polymer-assisted deposition[34–36] (PAD) using a complexation of polyethylene glycol (PEG)-V_2O_5 precursors.

Chemical synthesis, dip coating and a range of surface microscopies were used to analyze the film deposition process, structure, surface uniformity and the effects of different annealing treatments on the conversion process from stoichiometric V_2O_5 to a ternary metal oxide transparent thin film. Raman scattering and XPS measurements identified the composition during film formation and the development of visible transparency during annealing to a TTF. The influence of the precursor formulation and effect of higher viscosity polymer-assisted deposition using alkoxide-polyethylene glycol mixtures on the nature of the thin film coverage, uniformity and phase change process to a transparent ternary oxide film during different annealing treatment, was also studied.

We demonstrate how continuous annealing and interrupted (successive heating-cooling) annealing cycles influence the structure, morphology and broadband visible transparency during ternary TTF formation from V_2O_5 dip coated thin films.

Experimental

Precursor preparation and deposition.— Two types of vanadium pentoxide thin films were synthesized from vanadium (V) oxytriisopropoxide [$OV(OCH(CH_3)_2)_3$] purchased from Sigma-Aldrich. The alkoxide was mixed by volume with isopropyl alcohol (IPA) and water at a ratio of 1000:10:1 (IPA : alkoxide : H_2O) to produce a high concentration precursor. The same mixture ratio was applied when polyethylene glycol (PEG) was added instead of H_2O i.e. 1000:10:1 (IPA : alkoxide : PEG). To prevent hydrolysis prior to deposition, 4 Å molecular sieves were stored within the precursor.

Thin films were deposited onto the surface of the borosilicate glass substrates with a dip-coating technique using a PTL-MM01 desktop dip coater. A withdraw rate of 2.5 mm/s was used to deposit uniform thin films. The borosilicate glass substrates were cut to dimensions of 12 mm in length and 10 mm in width and then cleaned using an acetone, IPA and DI water wash prior to deposition and coating. To remove any organics present on the surface before and after deposition, the samples were UV-Ozone treated for 30 mins using a Novascan UV ozone system. Thin film samples were crystallized through thermal treatment in a conventional oven at the temperatures 300°C, 280°C and 250°C for a series of annealing times. A number of samples were also examined in an as-deposited state. For direct comparison to the TTF material, identical thin films of V_2O_5-H_2O were deposited in the same manner on commercial ITO coated substrates and annealed for 24 h at 300°C.

Dip-coating allows for little wastage of the liquid solution as during the deposition only the liquid which is to be converted through hydrolysis and condensation reactions is deposited on the substrate surface. The thickness of the solid thin film is then controlled by adjusting the liquid film which is deposited on the surface which can be altered through changes to the deposition rate, precursor solution alterations, and evaporation rate for a given surface, according to,[37–39]

$$h_0 = k_i \left(\frac{E}{Lu} + Du^{\frac{2}{3}} \right)$$

where h_0 is thin film thickness, k_i is the solution composition constant, E is the evaporation constant, L is the substrate width, u is the coating speed and D is the solution's physical/chemical characteristics.

Previously, the effect of PEG addition on the thickness of the thin films was examined for single and double dip-coated layers of V_2O_5 on ITO coated glass substrates. Each successive dip-coated layer of V_2O_5-H_2O and V_2O_5-PEG is ∼10–15 nm and 15–20 nm respectively.[40] The addition of PEG to the thin film results in an increase in thickness compared to a H_2O additive. The thickness for the 5 layer dip-coated V_2O_5-H_2O and V_2O_5-PEG thin film samples studied in this work are ∼50–60 nm and 70–80 nm, respectively, determined by AFM.

For analysis of optical transparency, each thin film was investigated after annealing intervals of 1, 6 and 24 h. Samples were annealed under two different conditions for these time-frames. One batch of thin films from each precursor was fabricated for annealing for each time period at subsequent annealing temperatures, e.g. 1 h at 300°C, and titled 'anneal'. A second batch of each film type was annealed at 1 h, cooled, then annealed to 6 h, subsequently cooled and finally annealed to a total of 24 h and referred to as 'anneal-cool'.

Thin film surface investigation.— Surface morphology was investigated using atomic force microscopy (AFM) using a Park XE-100 AFM system in non-contact mode with SSS-NCHR enhanced resolution tips. The XY and Z resolutions of the AFM system are ∼ 2 nm and ∼ 0.05 nm, respectively.

XPS spectra were collected on a Thermo Electron K-Alpha spectrometer using a monochromatic Al Kα X-ray source (1486.6 eV). Core level spectra from 100 scans were referenced to the C1s peak at 284.31 eV. The XPS spectra were processed using a Shirley background correction followed by peak fitting to Voigt profiles. The FWHM were allowed to vary within reasonable value ranges in order to achieve best fit.

Temperature-dependent optical transparency measurements.— Ultraviolet-visible spectroscopy was used to probe the optical transparency of the samples. A Thermo Scientific Evolution 60S UV-Visible spectrophotometer was used with a custom 3D printed sample holder under a Xenon light source in the 300 – 1000 nm range with a resolution of 0.5 nm. Raman scattering spectroscopy provided information on the molecular vibrations within the samples and was collected on a Renishaw InVia Raman spectrometer using a 514 nm 30 mW laser source. Spectra were collected using a RenCam CCD camera and the beam was focused onto the samples using either a 20× or 50× objective lens.

Results and Discussion

Surface morphology during conversion from V_2O_5 to transparent V-O-Na-Si TTF.— Two alternative vanadium pentoxide based thin films were synthesized and dip-coated onto glass substrates using a vanadium (V) oxytriisopropoxide based precursor with either a H_2O or PEG additive. The thin films were annealed at a range of different temperatures and at defined annealing times. The optical image in Fig. 1 shows the development of complete transparency in V_2O_5 due to the diffusion of SiO_2 and Na_2O species present within the borosilicate glass substrates, as we reported previously.[41] The AFM analysis presented in Figs. 1 and 2, outlines the influence of annealing conditions on the morphology and continuity of the films as they undergo the phase transition to the final $V_{0.0352}O_{0.547}Si_{0.4078}Na_{0.01}$ TTF phase.

The AFM surface images in Fig. 1 show the surface topography for as-deposited (non-annealed) V_2O_5 films from both diluted V_2O_5-H_2O (Fig. 1a) and V_2O_5-PEG precursors (Fig. 1b), and for both films after annealing at 250°C and 300°C for a period of 24 h. The as-deposited V_2O_5 is smooth and uniform, and the PAD film in Fig. 1b shows a lower roughness as a consequence of the polymer additive. We previously established that the PAD process still maintains a uniform coating of the V_2O_5 material after high-rate dip coating in the drainage regime.[40] During the crystallization process, the thin films undergo grain growth at 250°C and 300°C. PAD-assisted thin films are found to characteristically contain smaller grains during the annealing

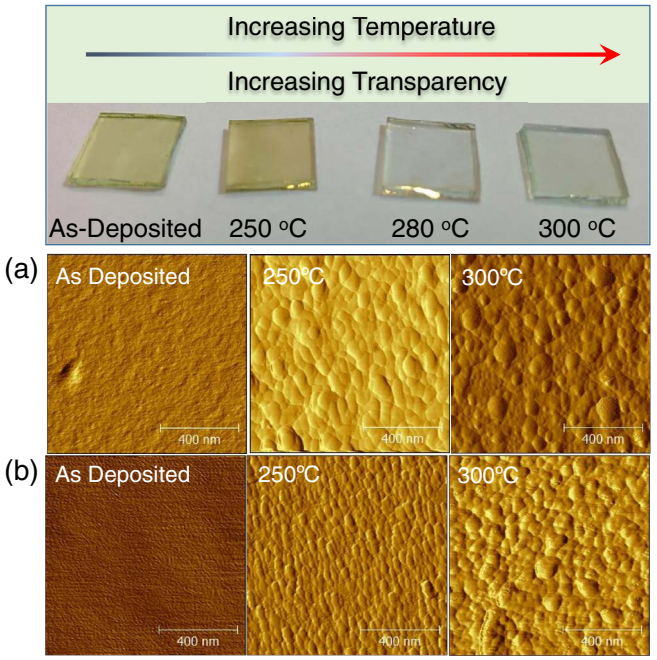

Figure 1. (Top) Optical images of as-deposited V_2O_5 thin films on glass, and the optical transparency development on conversion to a quaternary V-O-Na-Si TTF. (Bottom) AFM surface morphology images acquired for (a) V_2O_5-H_2O and (b) V_2O_5-PEG thin films at different temperatures.

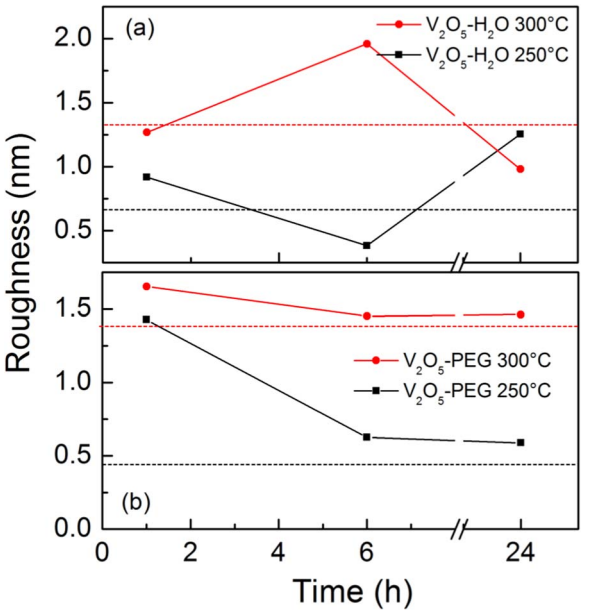

Figure 3. Variation of measured rms roughness as a function of annealing time for (a) V_2O_5-H_2O and (b) V_2O_5-PEG thin films at 250°C and 300°C. The dashed lines indicated the as-deposited rms roughness of the films prior to any annealing treatment.

conversion to a ternary oxide TTF, and the grain sizes are smallest at a higher density for conversion to V-O-Na-Si TTF when annealed at 300°C.

The AFM images in Fig. 2 show the development of the surface morphology after 1 h, 6 h, and 24 h during annealing at 300°C for (a) V_2O_5-H_2O and (b) V_2O_5-PEG thin films. In these measurements, the films are introduced to the annealing ovens after equilibration at the respective temperatures for the defined annealing time. These images also confirm that the grain boundary density increases with time as the phase conversion to a completely transparent TTF occurs during annealing. The V_2O_5-PEG thin films are characteristically smoother than the V_2O_5-H_2O thin films after annealing for each time period.

Figure 3 shows the differences in measured roughness values for each of the thin films as a function of annealing time at 250°C and 300°C. These roughness values were investigated for the two types of thin films for each temperature. In both cases, the thin films were generally smooth with low rms roughness values (< 2 nm). As shown in Fig. 3, the V_2O_5-PEG thin films exhibit a slightly rougher surface morphology at 300°C compared to the corresponding V_2O_5-H_2O thin films. However, the polymer-assisted dip-coated films of V_2O_5-PEG were found to be comparatively smoother than the corresponding V_2O_5-H_2O thin films at 250°C after 24 h with rms roughness values of 0.59 nm and 1.25 nm respectively. This also coincides with the observation that the V_2O_5-PEG AFM surface images show a higher concentration of crystalline grains than the V_2O_5-H_2O thin films owing to the complexation of the vanadium alkoxide precursor with PEG and the ability of the more viscous precursor to coat the substrate and avoid further roughness development during hydrolysis to V_2O_5.[19] Additionally, the rms roughness of the V_2O_5-PEG thin films did not vary substantially after 6 h of annealing, where the phase conversion process is incomplete and some patchy areas of the film begin to show optical clearing to a transparent film. These results show that the PAD processes in the PEG-based films allow for smoother surface morphology upon initial deposition, and allow the film to maintain a lower degree of rms roughness during the phase conversion process to a completely transparent thin film for each annealing temperature and time investigated.

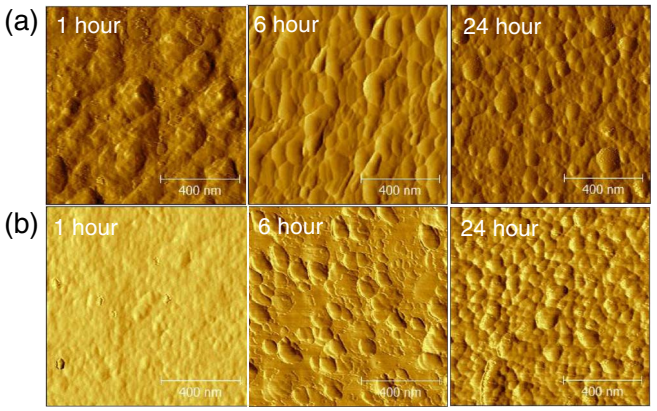

Figure 2. AFM surface images acquired after annealing for different time steps (1 h, 6 h and 24 h) for (a) V_2O_5-H_2O and (b) V_2O_5-PEG thin films.

Raman scattering and X-ray photoelectron spectroscopy of TTF composition.— Raman scattering spectroscopy was conducted to investigate the nature of the V_2O_5-H_2O and V_2O_5-PEG thin films from an as-deposited state to the formation of the crystalline TTF material. The distinct vibrational modes associated with the phase conversion to the crystalline TTF as a function of the annealing temperature and time was studied.

A direct comparison is also be made to identical V_2O_5-H_2O thin films deposited on an ITO coated glass substrate to show that the inter-diffusion of substrate and thin film species affects the formed thin film material. Raman scattering spectroscopy was performed on the stoichiometric and orthorhombic V_2O_5 thin films deposited on an ITO substrate as shown in Fig. 4a. Raman scattering spectra were also taken of bulk orthorhombic V_2O_5 for comparison. The characteristic V_2O_5 Raman vibrational modes are well known in the literature and are observed in thin films coated on the ITO substrate after the appropriate annealing time.[42,43] Prior to annealing, the stoichiometric V_2O_5 thin film shows no defined Raman peaks due to its amorphous structure.

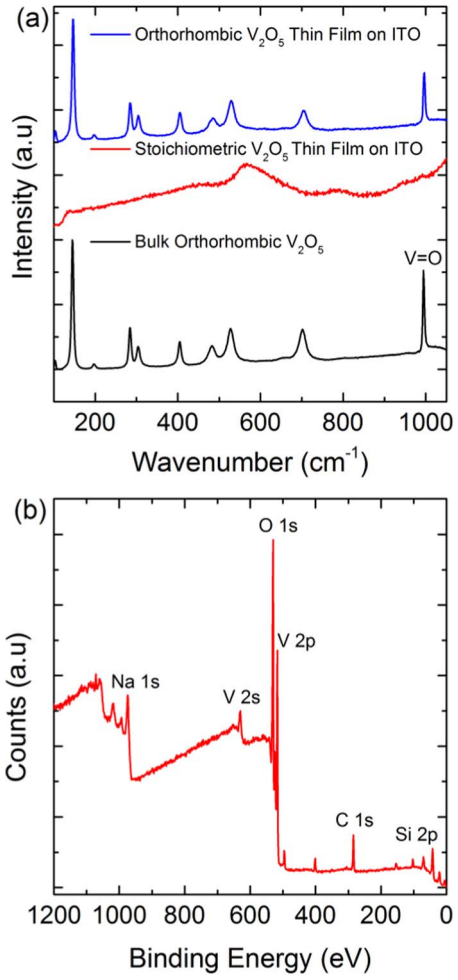

Figure 4. (a) Raman scattering spectroscopy of bulk V_2O_5, amorphous stoichiometric V_2O_5 on an ITO substrate and an annealed orthorhombic V_2O_5 thin film on an ITO substrate. (b) XPS measurement of stoichiometric V_2O_5 thin film on a borosilicate glass substrate prior to annealing.

The Raman mode located at 145 cm^{-1} is associated with the bilayer shearing of the V_2O_5 structure, this mode is indicative to the layering of the stacked V_2O_5 layers. The V = O mode at ~993 cm^{-1} is red-shifted to <1000 cm^{-1} due to the mixed valency of V^{4+}/V^{5+} within the material. The presence of the 145 cm^{-1} and the V = O mode in the Raman spectrum in Fig. 4a shows that the V_2O_5 thin film structure is the same as that of a bulk material but in a nanostructured thin film morphology. From the analysis of Fig. 4a ITO acts as a sufficient barrier layer to SiO_2 and Na-species diffusion.[40]

The Raman scattering spectrum of the V_2O_5-coated ITO substrate is also shown in Fig. 4a to demonstrate that there are no definitive peaks associated with the ITO. The as-deposited V_2O_5 is formed as amorphous nanoscale flakes of stoichiometric V_2O_5 during hydrolysis of the liquid precursor and sets into a thin film form, as previously reported in dedicated electron microscopy analysis.[19,40] These amorphous flakes do not show a defined Raman spectrum until they are crystallized during annealing to form orthorhombic V_2O_5 as seen in Fig. 4a. During the deposition of the thin films, it was shown previously how the formation of the amorphous flakes could be influenced by dewetting characteristics usually found in metal-polymer mixtures.[19,44–46] The application of the PAD technique results in the formation of smaller amorphous flakes with the added benefit of retarding the dewetting mechanism, resulting in a smoother surface with less surface discontinuities.[40]

An XPS measurement of an as-deposited thin film of V_2O_5 on a glass substrate was performed as shown in Fig. 4b. An amorphous

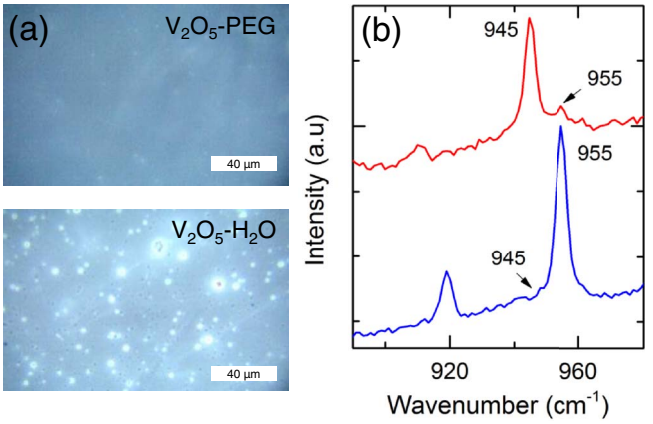

Figure 5. (a) Optical images and (b) corresponding Raman spectra of the resulting annealed films from V_2O_5-H_2O and V_2O_5-PEG precursors.

stoichiometric thin film of V_2O_5 was determined to be present on the substrate prior to annealing with the presence of both Si and Na species observed in the spectra caused by penetration of the X-rays and photoelectron emission through grain boundaries in the thin film that is significantly thicker (~70–80 nm) than beam penetration depth.[41] XPS at%. analysis has previously been performed to categorize the TTF material from the V_2O_5-H_2O precursor as a ternary mixed oxide phase $V_{0.0352}O_{0.547}Si_{0.4078}Na_{0.01}$ (after 24 h annealing). The incorporation of Si and Na are attributed to the species within the borosilicate glass substrate forming the TTF film after annealing through and inter-diffusion process.[41]

Optical surface images and Raman scattering spectra of the V_2O_5-PEG and V_2O_5-H_2O thin films after annealing are shown in Figs. 5a,5b respectively. Raman scattering spectra in Fig. 5b indicate a specific vibrational mode set that is indicative of the associated phase change for both V_2O_5-H_2O and V_2O_5-PEG thin films. They also do not coincide with a typical V_2O_5 phase,[40,43] confirming the diffusion of silicate and sodium oxide species from the glass in to the V_2O_5 film to form the V-O-Na-Si material. The Raman spectrum in Fig. 5b shows intense modes in the 915–960 cm^{-1} range that are only observed once transparency begins to develop. Concurrently, the characteristic V-O vibrational modes are replaced with Raman modes associated with bridged and non-bridged M-O (M = V, Si or Na) modes in the ternary oxide TTF.[41] The optical image of the thin films confirms the smoother overall morphology of the V_2O_5-PEG thin films. Importantly, Raman spectra confirmed that the TTF film is characterized by dominant modes at 955 and 918 cm^{-1}. In V_2O_5-PEG films, intermediate stages of phase conversion are characterized by a mode at 945 cm^{-1} (Fig. 5b) related to incomplete conversion to the final $V_{0.0352}O_{0.547}Si_{0.4078}Na_{0.01}$ TTF.

Optical transparency during annealing conversion to V-O-Na-Si TTF.— The optical characteristics of the thin films as a function of the annealing condition that led to the development of complete transparency as a ternary mixed metal oxide via phase conversion were acquired and shown in Figs. 6 and 7.

The optical transmittance measured in Fig. 6 shows the spectral response for the V_2O_5-H_2O thin films (left) and the V_2O_5-PEG films (right) taken at prescribed annealing time intervals heated at 250°C (a,b). Both sets of spectra, in general, show an increase in optical transmission as the films are annealed and the TTF is formed. The TTFs from V_2O_5-PEG thin films maintain a higher comparative overall transparency after each anneal-cool step at 250°C. An intermediate stage is always formed using V_2O_5-H_2O precursor thin films at 250°C as the TTF formation is initiated and the original VO thin film simultaneously undergoes crystallization. Polymer-assisted coatings of the V_2O_5-PEG thin films are smoother and generally more uniform. We previously showed that such films gelate from a nanofluid-like

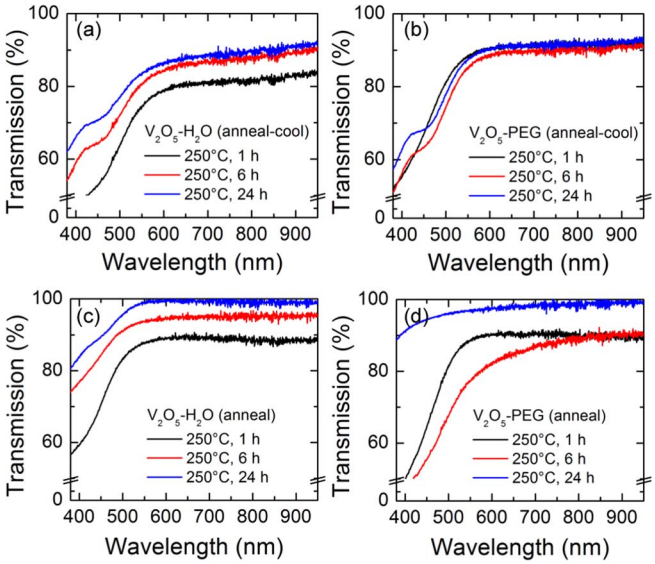

Figure 6. UV-Vis optical transmission spectra for (a,c) V_2O_5-H_2O and (b,d) V_2O_5-PEG thin films annealed at 250°C in order to convert to V-O-Na-Si TTF as a function of annealing time. Dip-coated thin films were treated with an anneal-cool (a,b) and a full anneal (c,d) protocol respectively (see Experimental).

solution containing a high density of constituent oxide flakes that densify upon annealing, but also allow for a higher rate of phase conversion to the V-O-Na-Si phase. This effect also increases interfacial reflectivity to lower the transmission. This latter process results in a lower transparency in the early (6 h or less) stages as the TTF has not fully formed through the inter-diffusion process. This intermediate stage at 250°C can be seen in the Fig. 1. When V_2O_5-PEG thins films are annealed, we note that the development of maximum transparency for that film at 250°C is more rapid under anneal-cool conditions. Under total annealing for the prescribed times (Figs. 6c,6d), transparency via phase conversion occurs to near complete optical clarity from V_2O_5-H_2O films at each time step is slightly higher than in the PEG-containing initial films, although consistent with all other data

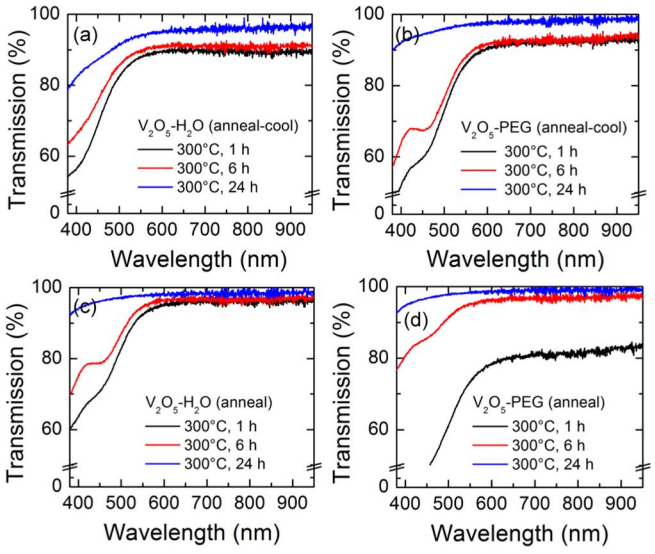

Figure 7. UV-Vis optical transmission spectra for (a, c) V_2O_5-H_2O and (b, d) V_2O_5-PEG thin films annealed at 300°C in order to convert to V-O-Na-Si TTF as a function of annealing time. Dip-coated thin films were treated with an anneal-cool and a full anneal protocol respectively (see Experimental).

shown in this work, the V_2O_5-PEG films after 24 h at 250°C exhibit the highest degree of transparency summed across the entire spectral range, including near-elimination of the strong absorption edge after 24 h total annealing (without intermittent cooling), compared to TTF from V_2O_5-H_2O-based films. This blueshift in the absorption edge is attributed to the formation of the TTF at a lower temperature than shown in the equivalent V_2O_5-H_2O thin film.

By comparison, the development of transparency during annealing at 300°C is somewhat similar for the V_2O_5-H_2O films under anneal-cool and full anneal conditions, and a similar degree of optical transmission enhancement is observed in both cases at 300°C (see Figs. 7a,7c). Fig. 7 shows that these films exhibit a greater degree of optical transparency after the 24 h annealing times, and in such films, greater increases in transparency are found from 6 h total annealing time. Intermittent anneal-cool treatment of the films eventually results in full transparency but significant increases are found after 6 h of this treatment. Overall, the response remarkably shows broadband visible transparency of almost 100% and greater than 90% from 380–1000 nm. In the range of 380–500 nm, an increase in optical transmittance of >20% is observed. We surmise that thermal energy required to melt, decompose and remove the PEG from the dip-coated film retards the rate of phase conversion compared to V_2O_5-H_2O films (*cf.* Fig. 5), and due to the nature of the sub-structure in polymer-assisted coatings, the eventual degree of transparency over a broader frequency range is greatest in these coatings.

Complete phase conversion to the V-O-Na-Si TTF is found after 24 h annealing at 300°C. As demonstrated, the optimum improvement in broader band visible transparency is found for the smoother PEG-assisted dip-coated thin films. We examined the transmittance at both 250°C and 300°C in both types of films at 450 nm (just slightly higher energy than the absorption edge) and at 900 nm where the highest visible transparency is noted. The data also includes the transmittance values for both types of films during conversion at both temperatures in either of the anneal or anneal-cool conditions.

The data shown in Fig. 8 summarizes the development of improved transmittance in both the V_2O_5-H_2O and V_2O_5-PEG thin films as they convert to the TTF during specific annealing conditions. In Figs. 8a,8c, we note that the smoother and more uniform polymer

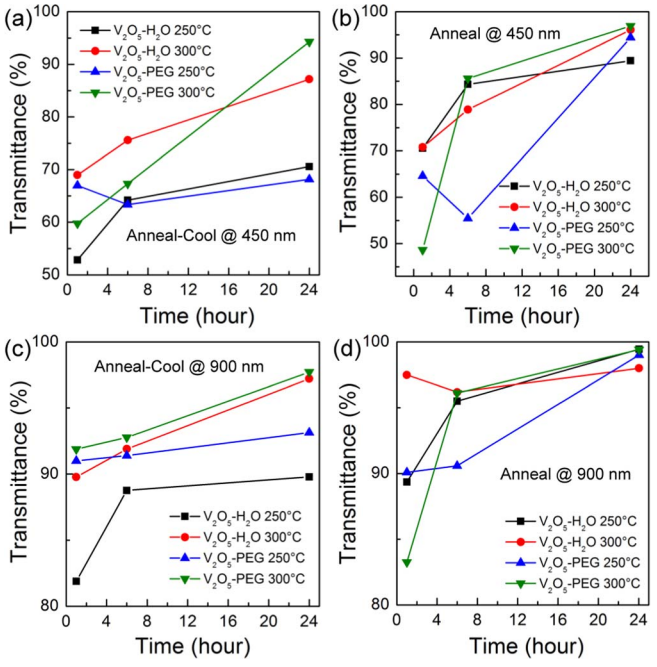

Figure 8. Transparency at 450 nm (a,b) and 900 nm (c,d) for both types of thin films annealed to the V-O-Na-Si TTF at 250°C and 300°C for 24 h under anneal-cool (left) and anneal (right) conditions.

assisted dip-coated films exhibit better overall visible transparency after 24 h of annealing due to the reduced size and higher density of V_2O_5 crystallite grains within the films. This morphology facilitates a faster rate of change to the TTF at a given temperature as indicated by the variation in effective absorption edge and transmittance at 450 nm. In Figs. 8b,8d, we find that the full annealing (without intermittent cooling) allows all films to develop optimum transparency after 24 h at both temperatures. All final TTF films exhibit between 82–96% transparency at 450 nm (below the absorption edge of V_2O_5), compared to ~50% at the absorption edge of the initial V_2O_5 film, under this annealing condition. The transparency at 450 nm is largely a function of the phase conversion process, since the absorption edge blue-shifts to values below 520 nm for the starting dip-coated V_2O_5 films.

In Figs. 8b,8d, the transmittance at 450 nm and 900 nm respectively was compared for all films at both temperatures as for Figs. 8a,8c. At 900 nm, all films including the starting V_2O_5 dip-coats, are nominally transparent to some degree at energies less than the absorption edge. At this wavelength, index contrast, scattering and reflection losses in addition to phase conversion also influence the total transmittance. We note in Fig. 8d, the PEG-based films again maintain the highest transparency at all temperatures during a full anneal (without intermittent cooling), and reach >90% within 1 h to >97% after 24 h. Overall, the thin films have high transparency at a broad range of wavelengths, and the nature of the TTF structure and optical constants of the resulting phase offer a broader frequency range for optical transparency with considerably higher overall transmittance.

The effective optical bandgap (E_g) of the V_2O_5 thin films can be approximated from a UV-Vis spectrum using a Tauc plot.[47] While the films are not entirely amorphous, indirect optical transitions relating to the comparative absorption edges in each film during the different annealing conditions that leads to the TTF formation, are possible.

The Tauc plots were calculated for the thin films heated at 250°C and 300°C (anneal-cool) at each time step measure (Fig. 9). The typical absorption edge energies for vanadium pentoxide thin films formed using the same procedure on ITO ranges from 2.18 eV to 2.69 eV.[40] For both types of V_2O_5 thin film, there are two distinct linear regions above the Urbach tail.[47] The higher E_g Tauc plot data for the V_2O_5-H_2O thin films shows a range of optical transitions from 3.393 eV to 3.546 eV, whereas the equivalent Tauc plot data for the annealed V_2O_5-PEG thin films ranges from 3.426 eV to 3.735 eV, and by comparison with Figs. 6 and 7, correlate to the increase in optical transparency via V-O-Na-Si conversion. The observed blue-shifting of the absorption edge during annealing is accompanied by a higher energy transition as the phase converts to a TTF. Importantly, the blueshift of the absorption edge and significant increase in transparency <500 nm is definitively due to the TTF formation.

This data shows a change in crystallization, increased transparency over a broader range of wavelengths, and the advantageous effect of polymer-assisted deposition on surface diffusion for the thin films. The PAD process was demonstrated to improve the quality of the deposit and surface uniformity.[19] The sol-gel process was used with the addition of the PEG to the precursor in this case but there are other processes that can be used with PAD such as liquid phase deposition (LPD), chemical bath techniques (CBT) and successive ion layer absorption and reaction (SILAR).[35] The PAD technique also allows for direct bonding controlled by the polymer, to offer better control of film uniformity, thickness and the possibility of thermally driven mixed metal doping to form an optically clear ternary metal oxide film.[16]

Conclusions

Fully transparent thin film ternary mixed metal oxide coatings were prepared on borosilicate glass through fast-rate dip-coating and the development of transparency was investigated as a function of the annealing condition. Hydrolyzed vanadium pentoxide-based precursor and polymer-assisted vanadium pentoxide-polyethylene glycol-based precursors were made to produce two different types of films to investigate the effects on surface morphology, composition on the optical

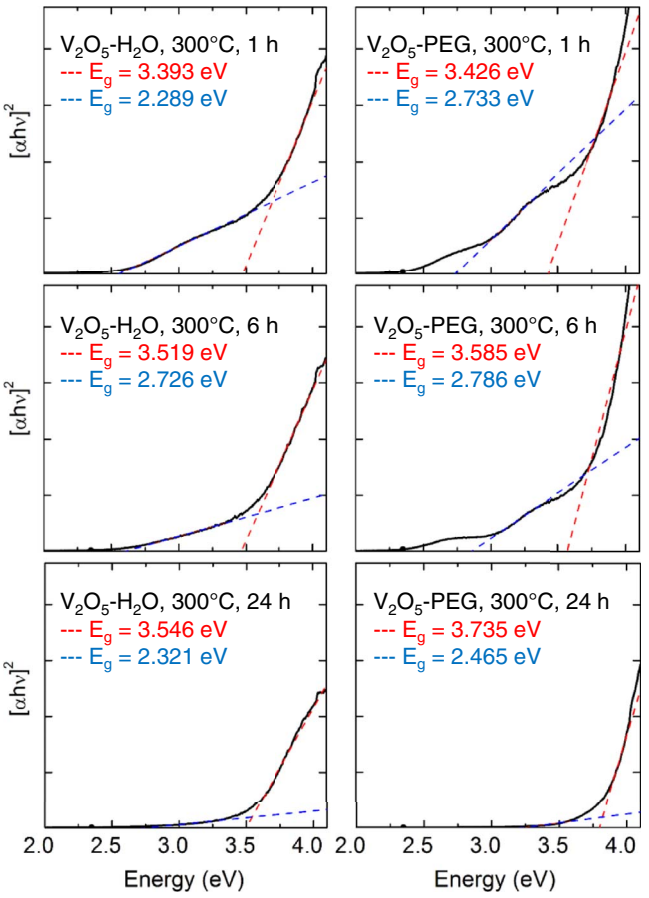

Figure 9. Tauc plots associated with the spectral data in Fig. 7. The value of E_g was calculated by extrapolating to $[\alpha h\omega]^2 = 0$ for both linear regions.

characteristics and eventual phase conversion to the V-O-Na-Si transparent thin film (TTF). The formation of the transparent oxide material through co-diffusion of vanadium oxide and Na-O and Si-O species on the borosilicate glass substrate was analyzed. ITO-coated glass was found to act as a diffusion barrier to prevent phase conversion to a TTF film. A comparative transparency range was found at both annealing temperatures after long treatment times (24 h). The addition of the PEG in V_2O_5-PEG high-rate dip-coated thin films resulted in a lower rms roughness and facilitated a faster rate of conversion to the TTF at all stages of annealing at both temperatures and under both anneal-cool and anneal conditions. Polymer-assisted dip-coated V_2O_5 films resulted in higher consistent visible transparency (> 95%) compared to the hydrolyzed vanadium pentoxide thin film across the full visible spectrum, with greater 90% transmission at <400 nm.

Acknowledgments

C.G. acknowledges the support of the Irish Research Council under award RS/2011/797. C.O.D. acknowledges support from the Irish Research Council New Foundations Award. This work was also supported by Science Foundation Ireland (SFI) under the National Access Programme (NAP 417), through an SFI Technology Innovation and Development Award under contract no. 13/TIDA/E2761. This publication has also emanated from research supported in part by a research grant from SFI under grant Number 14/IA/2581.

References

1. K. Nomura, H. Ohta, A. Takagi, T. Kamiya, M. Hirano, and H. Hosono, *Nature*, **432**, 488 (2004).
2. C. O'Dwyer, M. Szachowicz, G. Visimberga, V. Lavayen, S. B. Newcomb, and C. M. Sotomayor Torres, *Nat. Nanotechnol.*, **4**, 239 (2009).

3. R. A. Street, *Adv. Mater.*, **21**, 2007 (2009).
4. K. K. Banger, Y. Yamashita, K. Mori, R. L. Peterson, T. Leedham, J. Rickard, and H. Sirringhaus, *Nat. Mater.*, **10**, 45 (2011).
5. C.-P. Chen, Y.-D. Chen, and S.-C. Chuang, *Adv. Mater.*, **23**, 3859 (2011).
6. M. Alsawafta, A. Almoabadi, S. Badilescu, and V.-V. Truong, *J. Electrochem. Soc.*, **162**, H466 (2015).
7. M. A. Aegerter, C. O. Avellaneda, A. Pawlicka, and M. Atik, *J. Sol-Gel Sci. Technol.*, **8**, 689 (1997).
8. T. D. Manning, I. P. Parkin, M. E. Pemble, D. Sheel, and D. Vernardou, *Chem. Mater.*, **16**, 744 (2004).
9. C. G. Granqvist, *Thin Solid Films*, **564**, 1 (2014).
10. R. D. Chandra, M. Rao, K. Zhang, R. R. Prabhakar, C. Shi, J. Zhang, S. G. Mhaisalkar, and N. Mathews, *ACS Appl. Mater. Interfaces*, **6**, 773 (2014).
11. H. Ohta and H. Hosono, *Mater. Today*, **7**, 42 (2004).
12. C. Glynn, D. Thompson, J. Paez, G. Collins, E. Benavente, V. Lavayen, N. Yutronic, J. D. Holmes, G. Gonzalez, and C. O'Dwyer, *J. Mater. Chem. C*, **1**, 5675 (2013).
13. G. Gershinsky, H. D. Yoo, Y. Gofer, and D. Aurbach, *Langmuir*, **29**, 10964 (2013).
14. T. Paik, S.-H. Hong, E. A. Gaulding, H. Caglayan, T. R. Gordon, N. Engheta, C. R. Kagan, and C. B. Murray, *ACS Nano*, **8**(1), 797 (2014).
15. Z. Mao, W. Wang, Y. Liu, L. Zhang, H. Xu, and Y. Zhong, *Thin Solid Films*, **558**, 208 (2014).
16. T. Schneller, R. Waser, M. Kosec, and D. Payne, *Chemical Solution Deposition of Functional Oxide Thin Films*, p. 796, Springer, London (2013).
17. J. Boucle, P. Ravirajan, and J. Nelson, *J. Mater. Chem.*, **17**, 3141 (2007).
18. K. Zilberberg, S. Trost, J. Meyer, A. Kahn, A. Behrendt, D. Lützenkirchen-Hecht, R. Frahm, and T. Riedl, *Adv. Func. Mater.*, **21**, 4776 (2011).
19. C. Glynn, D. Creedon, H. Geaney, J. O'Connell, J. D. Holmes, and C. O'Dwyer, *ACS Appl. Mater. Interfaces*, **6**, 2031 (2014).
20. A. Carretero-Genevrier, G. L. Drisko, D. Grosso, C. Boissiere, and C. Sanchez, *Nanoscale*, **6**, 14025 (2014).
21. F. F. Lange, *Science*, **273**, 903 (1996).
22. D. R. Ceratti, B. Louis, X. Paquez, M. Faustini, and D. Grosso, *Adv. Mater.*, **27**, 4958 (2015).
23. S. Surnev, M. G. Ramsey, and F. P. Netzer, *Prog. Surf. Sci.*, **73**, 117 (2003).
24. F. Nicholas, M. P. Sean, W. H. Mark, and S. S. N. Bharadwaja, *J. Phys. D: Appl. Phys.*, **42**, 055408 (2009).
25. E. Skliri, I. Lykakis, and G. S. Armatas, *RSC Advances*, **4**, 46170 (2014).
26. E. Armstrong, M. Osiak, H. Geaney, C. Glynn, and C. O'Dwyer, *CrystEngComm*, **16**, 10804 (2014).
27. X. Liu, C. Huang, J. Qiu, and Y. Wang, *Appl. Surf. Sci.*, **253**, 2747 (2006).
28. C. O'Dwyer, V. Lavayen, D. A. Tanner, S. B. Newcomb, E. Benavente, G. González, and C. M. S. Torres, *Adv. Func. Mater.*, **19**, 1736 (2009).
29. J. Livage, *Materials*, **3**, 4175 (2010).
30. D. McNulty, D. N. Buckley, and C. O'Dwyer, *J. Electrochem. Soc.*, **161**, A1321 (2014).
31. D. McNulty, D. N. Buckley, and C. O'Dwyer, *J. Power Sources*, **267**, 831 (2014).
32. J. Livage, *Chem. Mater.*, **3**, 578 (1991).
33. H.-N. Cui, Preparation and characterization of optical multilayerd coating for smart windows applications. School of Sciences University of Minho (2005).
34. S. Yu, K. Yao, S. Shannigrahi, and F. T. E. Hock, *J. Mater. Res.*, **18**, 737 (2003).
35. Q. X. Jia, T. M. McCleskey, A. K. Burrell, Y. Lin, G. E. Collis, H. Wang, A. D. Q. Li, and S. R. Foltyn, *Nat. Mater.*, **3**, 529 (2004).
36. Y. D. Ji, T. S. Pan, Z. Bi, W. Z. Liang, Y. Zhang, H. Z. Zeng, Q. Y. Wen, H. W. Zhang, C. L. Chen, Q. X. Jia, and Y. Lin, *Appl. Phys. Lett.*, **101** (2012).
37. M. Faustini, D. R. Ceratti, B. Louis, M. Boudot, P.-A. Albouy, C. Boissière, and D. Grosso, *ACS Appl. Mater. Interfaces*, **6**, 17102 (2014).
38. M. Faustini, B. Louis, P. A. Albouy, M. Kuemmel, and D. Grosso, *J. Phys. Chem. C*, **114**, 7637 (2010).
39. D. Grosso, *J. Mater. Chem.*, **21**, 17033 (2011).
40. C. Glynn, D. Creedon, H. Geaney, E. Armstrong, T. Collins, M. A. Morris, and C. O. Dwyer, *Sci. Rep.*, **5**, 11574 (2015).
41. C. Glynn, D. Aureau, G. Collins, S. O'Hanlon, A. Etcheberry, and C. O'Dwyer, In Preparation (2015).
42. M. Castriota, N. Epervrier, T. Barone, G. De Santo, and E. Cazzanelli, *Ionics*, **13**, 205 (2007).
43. R. Baddour-Hadjean, A. Marzouk, and J. P. Pereira-Ramos, *J. Raman Spectrosc.*, **43**, 153 (2012).
44. H. C. Wong and J. o. T. Cabral, *Macromolecules*, **44**, 4530 (2011).
45. G. Amarandei, C. O'Dwyer, A. Arshak, U. Thiele, U. Steiner, and D. Corcoran, *Langmuir*, **29**, 6706 (2013).
46. R. Mukherjee, S. Das, A. Das, S. K. Sharma, A. K. Raychaudhuri, and A. Sharma, *ACS Nano*, **4**, 3709 (2010).
47. J. Tauc, *The Optical Properties of Solids*, Academic Press, New York (1966).